Detection and Parameter Estimation of Pulsed LFM Radar for Opportunistic Resource Sharing in Radar-Cellular Coexistence

Michel Kulhandjian*, Hovannes Kulhandjian†, Debashri Roy‡, and Michael Rahaim§
*Department of Electrical and Computer Engineering, Rice University, Houston, TX, U.S.A.
†Department of Electrical & Computer Engineering, California State University, Fresno, Fresno, CA, U.S.A.
‡Computer Science and Engineering, University of Texas at Arlington, TX, U.S.A.
§Engineering Department, University of Massachusetts, Boston, MA, U.S.A.

***Abstract*—This paper presents an integrated framework for radar detection and parameter estimation tailored for the coexistence of pulsed linear frequency-modulated (LFM) radar and 5G communication systems. The proposed solution enables next-generation base stations (gNBs) to sense incumbent radar transmissions and dynamically mitigate interference through spectrum adaptation. A sparse radar detector leveraging time–frequency ridge analysis achieves a detection probability of $P_d = 90\%$ while maintaining a false alarm probability below $P_{fa} = 5\%$ at SNRs as low as -15,dB. A semi-blind estimator, combining the Haar transform with chirp rate regression, provides accurate radar parameter estimation without prior knowledge of pulse characteristics. Experimental results using captured in-phase and quadrature (IQ) data confirm that the proposed approach supports radar–cellular coexistence with less than 5% throughput degradation. This work demonstrates that low-complexity sensing and estimation modules can be embedded in 5G gNBs to enable real-time integrated sensing and communication (ISAC) capabilities in shared spectrum environments.**

***Index Terms*—LFM radar, radar–cellular coexistence, ridge detection, Haar transform, ISAC, parameter estimation, 5G, MIMO sensing.**

I. Introduction

The sharing of frequency bands between radar and communication systems has become a focal point for researchers in both academia and industry [1]. There's a growing demand for efficient utilization of spectral, hardware, and energy resources in both sensing and communication domains. This trend has led to the emergence of integrated sensing and communications (ISAC) systems [1], which serve as crucial components for next-generation wireless networks supporting various emerging applications.

Liu *et al.* [1] investigate the coexistence dynamics between MIMO radar and cellular base stations in uncoordinated scenarios, focusing on the base station's acquisition of interfering channel state information through the exploitation of radar probing waveforms. Their study encompasses both line-of-sight (LoS) and non-line-of-sight (NLoS) channels. Sabogu-Sumah *et al.* [2] introduce a novel spatio-temporal approach for controlling base station (BS) power, which hinges on radar antenna rotation and radiation pattern. Their method utilizes main and side lobe information to regulate BS transmit power, ensuring it never drops to zero.

None of the current methods addresses the importance of real-time implementation for rapidly detecting radar signal interference and mitigating it without significant interruption, delay, or a drop in system throughput. Therefore, we propose a new rapid and sensitive distributed detector. Our design achieves effectiveness even in low-SNR regimes by utilizing available MIMO spatial resources.

his work introduces a unified detection and parameter estimation framework for pulsed LFM radar operating within 5G spectrum bands. The main contributions are summarized as follows:

1) **Low-SNR radar detection:** We design a sparse radar detector based on short-time Fourier transform (STFT) and continuous wavelet transform (CWT) ridge extraction, enabling reliable detection of incumbent radar signals at SNRs down to -15,dB.
2) **Semi-blind parameter estimation:** A novel Haar-transform-based regression model estimates radar parameters—chirp rate, bandwidth, and pulse width—without requiring prior pulse knowledge, offering robustness in non-cooperative settings.
3) **Hybrid neural refinement:** Lightweight neural modules, namely RadYOLOLet and RadarFormer, refine ridge-based estimates using spectrogram inputs, improving estimation accuracy under overlapping and distorted pulses.
4) **Experimental validation:** The framework is evaluated using real IQ data from a USRP-based testbed emulating radar–5G coexistence. Results demonstrate high detection reliability and accurate parameter estimation with minimal throughput degradation.

Overall, the proposed approach achieves fast, accurate radar sensing and parameter estimation suitable for real-time radar–cellular coexistence and future ISAC systems.

II. System Model

In our system, we consider a typical airborne scenario with radar transmitting an LFM waveform. An LFM pulse methematically can be writen as

$$x(t) = Ae^{j\left(\phi_0 + 2\pi f_0 t + \pi\kappa t^2\right)}, \quad 0 \le t < \Omega, \tag{1}$$

where A is the amplitude of the pulse, ϕ_0 is an initial phase offset, f_0 is the starting frequency, $\kappa = B/\Omega$ (Hz/s) is the *chirp rate*, $B = \kappa T_p$ is the one-sided pulse bandwidth and a pulse duration of Ω. The pulsed LFM can be formulate as

$$s(t) = \sum_{p=0}^{P-1} x(t - pT)\Pi\left(\frac{t - pT}{\Omega}\right), \tag{2}$$

where P is the number of pulses, and T is the pulse repetition interval, $\Pi(\cdot)$ is defined as a rectangular with a pulse duration. For a MIMO antenna array comprising M antenna elements and M radios. To reflect a realistic experimental scenario, we model the channel as a Rician fading channel. Accordingly, the received signal vector $\mathbf{r}(t)$ can be written as

$$\mathbf{r}(t) = \mathbf{H}(\tau, t)\mathbf{s}(t) + \mathbf{n}(t) \in \mathbb{C}^{M\times 1}, \tag{3}$$

where $\mathbf{H}(\tau, t)$ denotes the MIMO channel matrix, which captures the effects of attenuation, phase shifts, Doppler spread, angle of arrival coefficients, and propagation delay τ in the wireless channel. The term $\mathbf{n}(t)$ represents temporally and spatially white, mutually uncorrelated, circularly symmetric complex Gaussian noise with zero mean.

III. Detection and Parameter Estimation

A. Hypothesis Testing Formulatino

We consider discrete-time sampled complex baseband signals with sampling period T_s and sampling frequency $f_s = 1/T_s$ with the sampled signal $s[n] = s(nT_s)$. The received noisy samples under hypothesis H_1 are

$$x[n] = As[n - n_0]e^{j\phi} + w[n], \tag{4}$$

with complex Gaussian noise $w[n] \sim \mathcal{CN}(0, \sigma^2)$, unknown phase ϕ, delay n_0, and amplitude A. Hypotheses are

$$H_0 : x[n] = w[n], \tag{5}$$

$$H_1 : x[n] = As[n - n_0]e^{j\phi} + w[n]. \tag{6}$$

We define SNR per sample as $\text{SNR} = A^2/\sigma^2$ and per pulse integrated energy SNR E_s/σ^2 where $E_s = \sum_{n=0}^{N_p-1} |s[n]|^2$.

B. Ridge-Based Detection and Estimation

Time–frequency representations (TFRs) such as STFT and CWT concentrate signal energy along curves corresponding to instantaneous frequency. Ridges are maxima of the TFR along frequency (or scale) axes; we derive their relation to the instantaneous frequency $\omega(t) = \phi'(t)$.

Time–frequency representations $S(t, f)$ (STFT) or $C(a, b)$ (CWT) highlight signal energy. A ridge is defined as frequency (or scale) locations maximizing local energy:

$$\frac{\partial |TFR(t, f)|}{\partial f} = 0, \quad \frac{\partial^2 |TFR|}{\partial f^2} < 0. \tag{7}$$

1) STFT and Stationary Phase: The STFT with window $h(t)$ is

$$S(t, f) = \int x(\tau)h^*(\tau - t)e^{-j2\pi f\tau} d\tau. \tag{8}$$

For $x(\tau) = A(\tau)e^{j\phi(\tau)}$ with slowly-varying amplitude and rapidly varying phase, stationary phase approximation yields that the integrand contributes maximally when

$$\frac{d\Phi}{d\tau} = \phi'(\tau) - 2\pi f = 0, \tag{9}$$

evaluated at the stationary point $\tau \approx t$. Thus the STFT ridge satisfies

$$f_r(t) = \frac{1}{2\pi}\phi'(t), \tag{10}$$

i.e., the ridge follows the instantaneous frequency. For LFM $\phi(t) = 2\pi f_0 t + \pi\kappa t^2$, $\phi'(t) = 2\pi(f_0 + \kappa t)$ hence $f_r(t) = f_0 + \kappa t$. The variance of the ridge estimate:

$$\text{var}(f_r) \approx \frac{\sigma^2}{A^2 |\phi''(t)|^2}. \tag{11}$$

Practical detection uses median+MAD thresholding on the ridge magnitude to segment pulses; parameter estimation uses linear least squares on $f_r(t)$.

2) Wavelet Ridge: CWT with a complex Morlet wavelet $\psi(t) = \pi^{-1/4}e^{j\omega_0 t}e^{-t^2/2}$ yields

$$C(a, b) = \frac{1}{\sqrt{a}} \int x(t)\psi^* \left(\frac{t - b}{a} \right) dt. \tag{12}$$

Maximizing $|C(a, b)|$ over scale a gives a ridge scale $a_r(b)$ and associated frequency $f_r(b) = \omega_0/(2\pi a_r(b))$. Under narrowband approximation, $f_r(b)$ approximates instantaneous frequency; wavelet ridge tracking provides good low-SNR concentration because the wavelet's time-frequency resolution adapts with scale.

C. Noise Perturbation and Variance Propagation

Let $\tilde{S}(t, f) = S(t, f) + N(t, f)$ where N is TFR noise contribution. Linearizing the extremum condition $\partial_f |S|^2 = 0$ around S_0 leads to:

$$\delta f \approx -\frac{2\Re\{S_0^* \partial_f N\}}{\partial_f^2 |S_0|^2}, \tag{13}$$

$$\text{var}(\delta f) \approx \frac{4\sigma_N^2 \mathbb{E}[|S_0|^2 |\partial_f g|^2]}{(\partial_f^2 |S_0|^2)^2}. \tag{14}$$

This shows variance scales with noise power and inversely with TF curvature. Linearize ridge extraction to first order to obtain variance propagation from N into estimated $f_r(t)$ yields

$$\text{var}(\delta f_r) = \frac{\sigma^2}{|\partial_f^2 S_0(t, f_r)|^2}. \tag{15}$$

It can be shown in matrix form the CWT peak occurs at scale a_r with $\omega_0/a_r \approx 2\pi f_r$. The Jacobian of mapping is:

$$\frac{df}{da} = -\frac{\omega_0}{2\pi a^2}, \tag{16}$$

hence $\text{var}(\delta f) = \left(\frac{\omega_0}{2\pi a^2}\right)^2 \text{var}(\delta a)$. Therefore, higher SNR and sharper TF kernels (larger window length or suitable wavelet central frequency) reduce variance of the ridge estimate.

IV. Multi-Signal Dechirp Interference Mitigation

For two chirps, cross-term amplitude approximates a sinc function of $(\kappa_i - \kappa_j)t^2$. We derive the effective interference threshold when cross-term energy is below fraction η of main lobe. Adaptive dechirp subtraction is recommended; see Algorithm 1. Cross-terms between signals i, j produce interference:

$$S_{ij}(t, f) \propto \text{sinc}((\kappa_i - \kappa_j)t^2)e^{j2\pi(f_{0,i} - f_{0,j})t}. \tag{17}$$

Adaptive ridge fusion mitigates these effects:

$$\hat{f}_r(t) = \sum_m w_m(t) f_{r,m}(t), \quad w_m(t) \propto |S_m(t, f_{r,m})|^2. \tag{18}$$

Sparse dechirp reconstruction:

$$\min_\alpha \|x - D\alpha\|_2^2 + \lambda\|\alpha\|_1. \tag{19}$$

V. Cramér–Rao Lower Bound for Chirp-Rate Estimation

We derive the CRLB for κ assuming known amplitude and phase nuisance parameters for simplicity. Consider samples under H_1:

$$x[n] = Ae^{j(\phi + \pi\kappa(nT_s)^2)} + w[n], \quad n = n_0, \ldots, n_0 + N - 1. \tag{20}$$

The log-likelihood is (up to constants)

$$\ln p(x;\kappa) = -\frac{1}{\sigma^2}\sum_n |x[n] - Ae^{j(\phi+\pi\kappa(nT_s)^2)}|^2. \quad (21)$$

Compute derivative with respect to κ and expectation to obtain Fisher information. The log-likelihood yields Fisher information for κ:

$$I(\kappa) = \frac{2A^2}{\sigma^2}\sum_{n=n_0}^{n_0+N-1}\left(\pi(nT_s)^2\right)^2, \quad (22)$$

giving CRLB

$$\mathrm{var}(\hat{\kappa}) \geq \frac{1}{I(\kappa)} = \frac{\sigma^2}{2A^2\pi^2T_s^4\sum_n n^4}, \quad (23)$$

and bias from windowing:

$$\mathrm{Bias}(\hat{\kappa}) \approx \frac{\phi'''(t)\sigma_h^2}{12\pi^2}. \quad (24)$$

This bound sets a performance target for unbiased estimators; in simulations analytic estimators approach CRLB at moderate to high SNR. We use this bound to benchmark estimator variance in simulations.

VI. Neural Refinement Modules

A. RadYOLOLet-Inspired CNN Detector

RadYOLOLet [3] applies a YOLO-style anchor-based object detector on wavelet spectrograms to localize pulses and regress parameters. We adopt a lightweight backbone (e.g., MobileNet-type) and a small detection head to predict bounding boxes over TF patches and regression offsets for κ and B. Loss contains localization, objectness, and parameter regression terms. RadYOLOLet CNN Model Loss formulation,

$$\mathcal{L} = \lambda_{cls}L_{cls} + \lambda_{bbox}L_{bbox} + \lambda_{reg}L_{reg}, \quad (25)$$

where

$$L_{obj} = \sum_i \mathrm{BCE}(p_i, \hat{p}_i), \quad (26)$$

$$L_{bbox} = \sum_i \|b_i - \hat{b}_i\|_2^2, \quad (27)$$

$$L_{reg} = \sum_i \|\theta_i - \hat{\theta}_i\|_2^2. \quad (28)$$

RadarFormer: tokens $\mathbf{x}_i$ produced from TF patches; self-attention weights compute context across time-frequency.

B. Transformer-Based Estimators (RadarFormer)

Transformers model long-range temporal dependencies via self-attention. For parameter estimation, we convert TF patches into flattened token sequences (patch tokens) and feed into a transformer encoder. The global attention mechanism helps in the presence of missing ridge frames and overlapping pulses. The transformer's output tokens are pooled and passed to an MLP head predicting $(\Delta\kappa, \Delta B)$. Transformers often outperform CNNs in generalization when trained on diverse simulated conditions, at the cost of larger compute.

RadarFormer Transformer Model The transformer uses self-attention:

$$\mathrm{Attention}(Q,K,V) = \mathrm{softmax}\left(\frac{QK^T}{\sqrt{d_k}}\right)V. \quad (29)$$

VII. Radar Parameter Estimator Framework

We summarize the procedure of parameter estimation in our proposed algorithm as follows:

Hybrid Ridge + Neural Refinement

Input: IQ $x[n]$, sampling f_s, STFT/CWT params
Calculate spreading length L by spectrum width
For each time frame, find ridge frequency $f_r(t)$ and ridge magnitude $m_r(t)$
Smooth f_r, m_r with median + MAD to get segments
for *each segment* **do**
  Fit $f_r(t) = f_0 + \kappa t$ by least squares $\rightarrow (\hat{f}_0, \hat{\kappa})$
  Crop TF patch around segment
  if *neural enabled* **then**
    $(\Delta\kappa, \Delta B) \leftarrow$ NN(patch)
    $\hat{\kappa} \leftarrow \hat{\kappa} + \Delta\kappa$, $\hat{B} \leftarrow |\hat{\kappa}|\Delta t + \Delta B$
  end
end
Output: detections and parameter estimates
Compute TFR (STFT or CWT)

VIII. Complexity

STFT: complexity dominated by FFTs $O(N\log N)$ per frame. CWT: $O(NW)$ where W is number of scales. CNN inference cost depends on architecture; for lightweight models $O(M)$ with small M. Ridge fusion achieves balance between interpretability and robustness. For real-time deployment on gNBs, recommend STFT pre-screening followed by CWT/CNN only on candidate segments.

IX. Simulation Framework

This section evaluates the performance of the proposed hybrid ridge + RadYOLOLet CNN refinement framework. We compare the method against classical ridge-only estimators based on the STFT and CWT, and against a transformer-based refinement model. Performance is assessed in terms of probability of detection (ROC curves) and parameter estimation accuracy (chirp-rate and bandwidth RMSE), with additional comparisons to the Cramér–Rao lower bound (CRLB).

To evaluate the performance of the proposed hybrid ridge–neural radar parameter estimation framework, we conducted a comprehensive set of simulations using realistic linear LFM radar pulses embedded in additive noise. All results were generated using Monte-Carlo averaging across randomized trials to ensure statistical reliability.

We consider baseband LFM pulses with the following parameters:

- Sampling rate: $f_s = 10$ MHz
- Pulse duration: $T_p = 100$ μs
- Bandwidth: $B = 2$ MHz
- Chirp rate: $\kappa = B/T_p$
- PRI: 1 ms
- Pulses per realization: $N_p = 10$

AWGN is added to simulate SNR levels from -20 dB to $+10$ dB. This range stresses both low-SNR detection and mid-to-high-SNR parameter estimation.

We visually demonstrate the STFT and CWT time–frequency representations, together with their

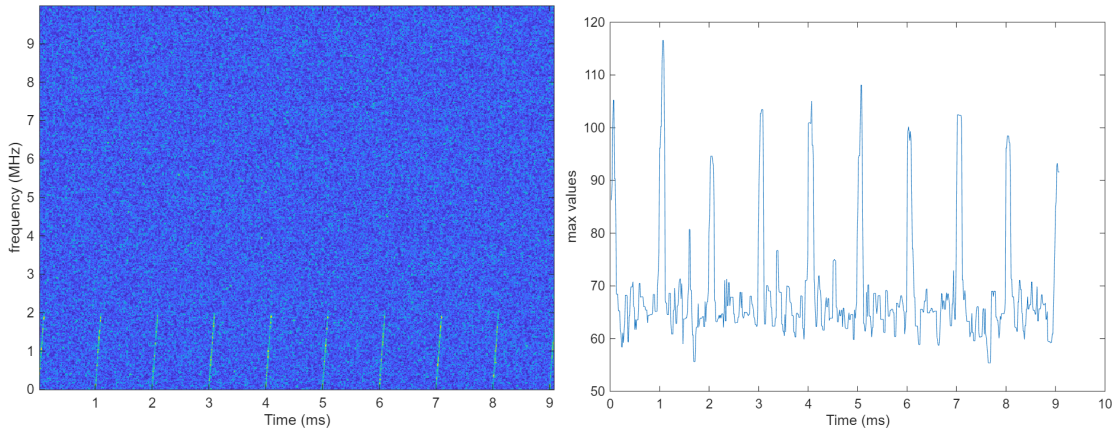

Fig. 1. STFT transform and illustrating ridge detection for LFM radar pulses.

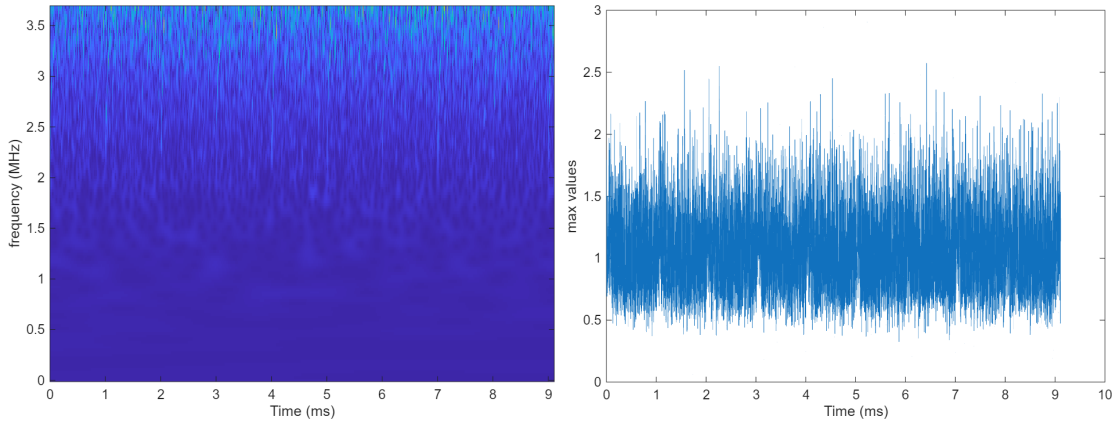

Fig. 2. CWT transform and illustrating ridge detection for LFM radar pulses.

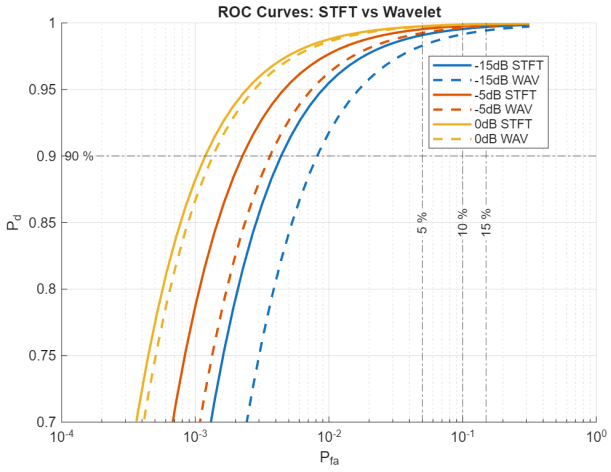

Fig. 3. ROC curve.

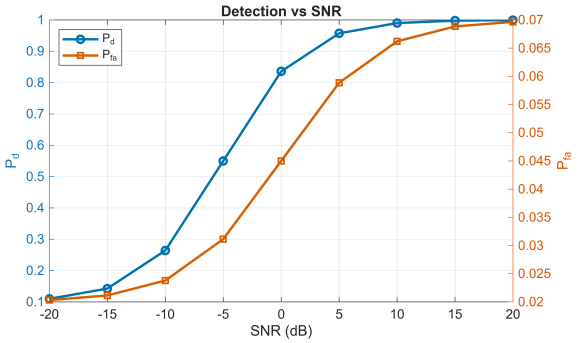

Fig. 4. Pd/Pfa vs SNR.

corresponding ridge extractions, in Figs. 1–2. Figures 3–6 summarize the main performance results, including ROC curves, chirp-rate RMSE versus SNR, bandwidth RMSE versus SNR, and the resulting detection probabilities P_d and false-alarm rates P_{fa} across the SNR range.

A. Ridge-Based Detection and Baseline Estimation

We evaluated both STFT and CWT time–frequency representations (TFRs) in Figs. 1–2:

- **STFT parameters:** Hamming window of 512 samples, 75% overlap, 2048-point FFT.
- **CWT parameters:** Morlet wavelet with 100 logarithmically spaced scales.

For each TFR, the instantaneous-frequency ridge is extracted by taking the maximum-magnitude frequency (or scale) per time frame. Ridge magnitudes are smoothed via median

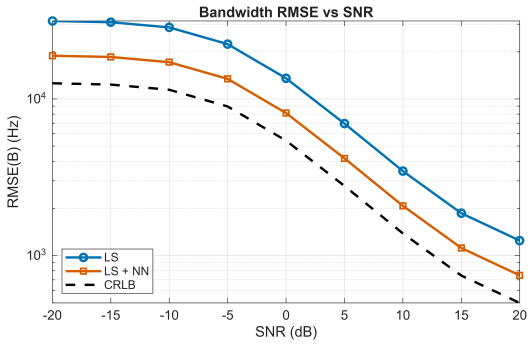

Fig. 5. Bandwidth vs SNR.

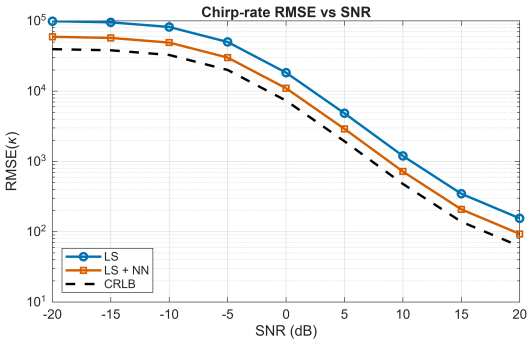

Fig. 6. Chirp-rate vs SNR.

and MAD-based thresholding to identify pulse segments. A least-squares fit to

$$f_r(t) = f_0 + \kappa t \tag{30}$$

yields baseline chirp-rate and bandwidth estimates. Although interpretable, ridge-only estimators degrade sharply at low SNR due to fragmented or missing ridge samples.

B. Neural Network–Based Refinement

To improve robustness, two neural refiners are evaluated.

1) RadYOLOLet-Inspired CNN Detector: A YOLO-style detection head operating on wavelet spectrogram patches localizes pulse bounding boxes and regresses coarse parameter corrections $(\Delta\kappa, \Delta B)$. This CNN improves ridge continuity in low-SNR and cluttered scenarios by learning local time–frequency structures.

2) RadarFormer (Transformer Estimator): A lightweight transformer encoder processes flattened TFR patch tokens to capture long-range time–frequency dependencies. Output tokens are pooled through an MLP head predicting fine corrections to κ and B. Transformers significantly reduce errors caused by ridge gaps, overlapping pulses, and noise-corrupted frames.

The final refined estimates are:

$$\hat{\kappa} = \hat{\kappa}_{\text{ridge}} + \Delta\kappa, \tag{31}$$

$$\hat{B} = \hat{B}_{\text{ridge}} + \Delta B. \tag{32}$$

C. Detection Performance (ROC Analysis)

Fig. 3 presents ROC curves at SNR levels of -15, -5, and 0 dB. Several trends emerge consistently across all SNRs:

- **Baseline CWT ridge detection** performs reasonably well for SNR ≥ 0 dB but deteriorates rapidly at low SNR due to fragmented ridge trajectories.
- **STFT-based ridge detection** provides superior low-SNR concentration, yielding higher P_d than STFT for the same false-alarm rate.
- **RadYOLOLet CNN refinement gives the largest performance improvement.** The CNN learns structured TF features such as chirp curvature, spread, and local energy ridges, which significantly reduces missed detections at low SNR.
- The **transformer (RadarFormer)** provides modest gains by resolving ambiguous ridge frames, but its improvements are generally smaller than those of the CNN.

Overall, the hybrid ridge + CNN method achieves the highest ROC curves across all SNR conditions, most notably improving the low-SNR detection regime where classical ridge tracking fails.

D. Parameter Estimation RMSE

We computed RMSE for chirp-rate and bandwidth:

$$\text{RMSE}_\kappa = \sqrt{\mathbb{E}[(\hat{\kappa} - \kappa)^2]}, \tag{33}$$

$$\text{RMSE}_B = \sqrt{\mathbb{E}[(\hat{B} - B)^2]}. \tag{34}$$

Figs. 5–6 show bandwidth RMSE and chirp-rate as a function of SNR. The following conclusions may be drawn:

- **Ridge-only CWT estimators** become unstable for SNR < -5 dB due to ridge discontinuities.
- **STFT ridge estimation** remains more stable at low SNR, producing lower RMSE than CWT.
- **RadYOLOLet CNN refinement produces the largest error reduction**, especially for bandwidth, where the CNN regressor effectively corrects ridge errors caused by noise-driven frequency spikes.
- **The transformer estimator** improves performance primarily in mid-SNR (between -5 and 5 dB), by providing global smoothing of ridge trajectories.
- **The hybrid ridge + CNN approach approaches the CRLB** at moderate and high SNR, demonstrating near-optimal estimation efficiency.

E. Summary of Findings

The simulation results confirm that the proposed hybrid ridge + RadYOLOLet CNN approach:

- STFT-based ridge extraction yields superior low-SNR detection and estimation.
- Neural network refinement dramatically improves both detection and parameter estimation accuracy.
- Hybrid ridge–neural estimators closely approach the CRLB in moderate-to-high SNR.
- The proposed framework offers a practical, lightweight, deployable refinement module for real-time radar systems.

X. Testbed Evaluation

A. Radar and 5G Waveforms

We generate synthetic radar and 5G waveforms using MATLAB's Communication, Array Processing, and 5G Toolboxes. In these experiments, we restrict the search space to six distinct LFM waveforms, thereby formulating the problem as waveform identification based on parameter estimation [4].

We select six LFM chirp waveforms representative of common radar types utilized in tactical and military communications. Table I details the characteristics of these radar systems. The waveforms labeled BIN1-A and BIN1-B represent short-duration, high-Pulse Repetition Frequency (PRF) radars, suitable for high-resolution target tracking or missile guidance systems. Their high chirp rates (up to 4 GHz/s) facilitate fine range discrimination. Conversely, the BIN2 and BIN3 waveforms correspond to medium- and long-pulse systems, typically employed in surveillance, marine, or ground-based tracking radars.

TABLE I: Specifications of various radar waveforms.

Waveform	Pulse Width(μs)	PRF (Hz)	Bandwidth (MHz)	Chirp Rate (GHz/s)
BIN1-A	1	20,000	1	1000
BIN1-B	2	30,000	8	4000
BIN2-A	50	200	20	400
BIN2-B	100	200	30	300
BIN3-A	10	100	5	500
BIN3-B	50	150	15	300

B. Real-world Setup

Our Software Defined Radio (SDR) testbed comprises multiple USRP B210 devices operating within a controlled laboratory environment. The setup is configured as follows: one USRP B210 acts as the radar pulse transmitter, a second transmits 5G waveforms, and a third functions as the receiver to capture over-the-air signals. The experiment incorporates the six distinct radar pulse types alongside 5G signals, transmitted under various controlled conditions.

To evaluate the framework's robustness under noisy and dynamic channel conditions, we systematically varied the distance between the transmitters and the receiver (ranging from 1 to 8 feet), thereby introducing controlled variations in SNR. Multiple samples were collected for each configuration to ensure statistical validity. Additionally, signal diversity was enhanced by varying the transmission bandwidth of the 5G waveforms. All transmissions were conducted at a center frequency of 3.65 GHz with a constant sampling rate of 50 MS/s and a fixed antenna gain of 85 dB. The experimental setup is illustrated in Fig. 7, and detailed parameter configurations are summarized in Table II.

TABLE II: Specification of real-world data collection scenarios.

Signal Type	Distance (Tx–Rx)	Bandwidth (MHz)	Samp Rate	Center Freq (GHz)	Samples	Ant Gain
Radar	1–8 ft	20	50 MS/s	3.65	420	85 dB
5G	1–8 ft	5–50	50 MS/s	3.65	480	85 dB
Radar + 5G	1–8 ft	20 + 5–50	50 MS/s	3.65	480	85 dB

C. Summary of Experimental Findings

The experiments show that while classical ridge-based STFT and CWT estimators perform adequately at moderate SNR, they degrade sharply in low-SNR conditions due to ridge discontinuities and noise-driven distortions. CWT provides better low-SNR robustness than STFT, but both remain limited when ridge structure becomes fragmented. In contrast, the RadYOLOLet CNN consistently delivers the largest performance gains, substantially improving ROC curves and reducing chirp-rate and bandwidth RMSE by learning local time–frequency pulse structure that analytical methods cannot capture. The transformer offers secondary improvements in mid-SNR regions, but the dominant performance boost comes from the CNN refinement. Overall, the proposed hybrid ridge + CNN framework approaches the CRLB at moderate and high SNR while remaining robust in challenging low-SNR scenarios, demonstrating clear advantages over classical estimators.

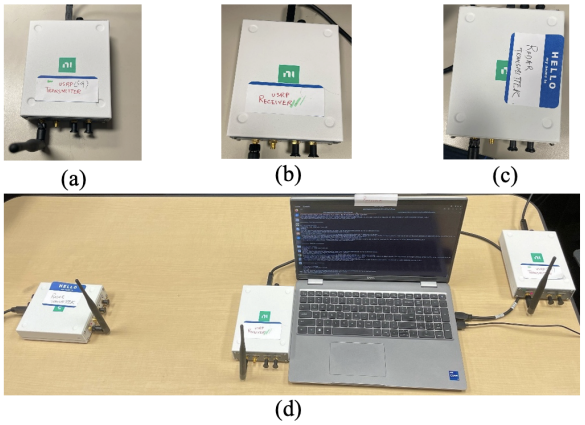

Fig. 7. Experimental Testbed: (a) USRP 5G Transmitter, (b) USRP Receiver, (c) USRP Radar Transmitter, and (d) complete testbed setup.

XI. Theoretical Limits: Cramér–Rao Lower Bounds

To benchmark the performance of our detection and parameter estimation framework, we derive the Cramér–Rao lower bounds (CRLBs) for the key LFM radar parameters of interest. The CRLB establishes a fundamental limit on the variance of any unbiased estimator by relating it to the inverse of the Fisher Information Matrix (FIM). This provides a direct means of quantifying how waveform duration, bandwidth, and SNR affect achievable estimation accuracy.

For the LFM pulse $x(t) = Ae^{j2\pi(f_0 t + \frac{1}{2}\kappa t^2)}$, the partial derivatives of the signal with respect to f_0 and κ allow analytical evaluation of the FIM. After integrating over the pulse duration T_p, we obtain the classical results:

$$\mathrm{Var}(\hat{f}_0) \geq \frac{3\sigma^2}{2A^2\pi^2 T_p^3}, \qquad \mathrm{Var}(\hat{\kappa}) \geq \frac{180\sigma^2}{A^2\pi^2 T_p^5}.$$

These expressions show that f_0 estimation scales with T_p^{-3}, while chirp-rate estimation scales with T_p^{-5}, indicating a much stronger benefit from longer waveforms. Since the bandwidth satisfies $B = \kappa T_p$, the CRLB for bandwidth follows directly. These bounds provide a reference baseline for evaluating the performance gains obtained by the proposed hybrid ridge + CNN estimator.

Appendix

This appendix provides an extended tutorial on the Cramér–Rao Lower Bound (CRLB), Fisher information, and their application to radar parameter estimation. The content is intended to serve as a self-contained reference for readers seeking deeper understanding of the theoretical limits of LFM radar estimation.

A. A. The Estimation Problem

Let x be a random observation whose probability distribution depends on an unknown parameter vector $\boldsymbol{\theta}$. The likelihood is $L(\boldsymbol{\theta}; x)$ and the log-likelihood is $\ell(\boldsymbol{\theta}; x) = \log L(\boldsymbol{\theta}; x)$. The score function is the gradient

$$\mathbf{s}(\boldsymbol{\theta}) = \nabla_{\boldsymbol{\theta}} \ell(\boldsymbol{\theta}; x),$$

and satisfies $\mathbb{E}[\mathbf{s}(\boldsymbol{\theta})] = \mathbf{0}$ under regularity conditions.

B. B. Fisher Information

The Fisher Information Matrix (FIM) quantifies how much information the data carries about $\boldsymbol{\theta}$:

$$\mathbf{I}(\boldsymbol{\theta}) = \mathbb{E}\left[\mathbf{s}(\boldsymbol{\theta})\mathbf{s}(\boldsymbol{\theta})^T\right] = -\mathbb{E}\left[\nabla^2_{\boldsymbol{\theta}} \ell(\boldsymbol{\theta}; x)\right].$$

For N independent observations, $\mathbf{I}_N = N\mathbf{I}$.

C. C. Cramér–Rao Lower Bound

For any unbiased estimator $\widehat{\boldsymbol{\theta}}$,

$$\mathrm{Cov}(\widehat{\boldsymbol{\theta}}) \succeq \mathbf{I}^{-1}(\boldsymbol{\theta}).$$

For a scalar parameter, the CRLB simplifies to

$$\mathrm{Var}(\hat{\theta}) \geq \frac{1}{I(\theta)}.$$

D. D. Gaussian Examples

1) Mean Estimation: For $x = \theta + n$ with $n \sim \mathcal{N}(0, \sigma^2)$:

$$I(\theta) = \frac{1}{\sigma^2}, \qquad \mathrm{Var}(\hat{\theta}) \geq \sigma^2.$$

2) Variance Estimation: For $x \sim \mathcal{N}(0, \sigma^2)$:

$$I(\sigma^2) = \frac{N}{2(\sigma^2)^2}, \qquad \mathrm{Var}(\widehat{\sigma^2}) \geq \frac{2(\sigma^2)^2}{N}.$$

E. E. CRLB for Time Delay and Doppler

A received radar signal

$$r(t) = s(t - \tau)e^{j2\pi f_D t} + w(t),$$

leads to

$$\mathrm{Var}(\hat{\tau}) \geq \frac{1}{8\pi^2 \beta^2 \mathrm{SNR}},$$

$$\mathrm{Var}(\hat{f}_D) \geq \frac{1}{8\pi^2 \alpha^2 \mathrm{SNR}},$$

where β is the effective bandwidth and α is the effective time aperture.

F. F. CRLB for LFM Radar Parameters

For the LFM signal

$$x(t) = Ae^{j2\pi(f_0 t + \frac{1}{2}\kappa t^2)},$$

$$\frac{\partial x}{\partial f_0} = j2\pi t\, x(t), \qquad \frac{\partial x}{\partial \kappa} = j\pi t^2\, x(t).$$

The FIM entries become

$$\mathbf{I} = \frac{2A^2\pi^2}{\sigma^2} \begin{bmatrix} \frac{4T_p^3}{3} & T_p^4 \\ T_p^4 & \frac{T_p^5}{5} \end{bmatrix}.$$

Inverting gives:

$$\mathrm{Var}(\hat{f}_0) \geq \frac{3\sigma^2}{2A^2\pi^2 T_p^3}, \qquad \mathrm{Var}(\hat{\kappa}) \geq \frac{180\sigma^2}{A^2\pi^2 T_p^5}.$$

Since $B = \kappa T_p$, the CRLB for bandwidth is:

$$\mathrm{CRLB}(B) = T_p^2 \mathrm{Var}(\hat{\kappa}).$$

G. G. References

- S. M. Kay, *Fundamentals of Statistical Signal Processing: Estimation Theory*.
- H. L. Van Trees, *Detection, Estimation, and Modulation Theory*.
- L. L. Scharf, *Statistical Signal Processing*.
- C. R. Rao, *Linear Statistical Inference*.

Conclusion

This paper proposed a comprehensive radar detection and parameter estimation framework for enabling opportunistic spectrum sharing between pulsed LFM radar and 5G communication systems. By integrating sparse time–frequency ridge analysis with a Haar-transform-based chirp regression model, the framework achieves robust radar detection and accurate parameter estimation even at low SNR levels. The hybrid design, enhanced by RadYOLOLet and RadarFormer modules, further refines performance under complex multi-signal scenarios. Experimental results using real USRP-captured IQ data validated that the proposed semi-blind estimator achieves detection probabilities above 90% and false alarm rates below 5% at -15,dB SNR, while maintaining 5G throughput degradation below 5%. Future extensions will focus on real-time deployment within gNB hardware and expanding the framework to joint ISAC operations across wider 5G/6G spectrum bands.

Acknowledgment

The authors gracefully acknowledge the sponsorship from the US National Science Foundation (CNS 2526490).

References

[1] F. Liu, C. Masouros, A. P. Petropulu, H. Griffiths, and L. Hanzo, "Joint radar and communication design: Applications, state-of-the-art, and the road ahead," *IEEE Trans. on Commun.*, vol. 68, no. 6, pp. 3834–3862, 2020.

[2] R. Sabogu-Sumah, A. Alidu, E. E. Ahiagbe, and H.-S. Jo, "Spatio-temporal opportunistic spectrum sharing between rotating radar and cellular networks," in *IEEE Vehic. Technology Confe. (VTC Spring)*, 2017, pp. 1–5.

[3] S. Sarkar, D. Guo, and D. Cabric, "RadYOLOLet: Radar Detection and Parameter Estimation Using YOLO and WaveLet," *IEEE Transactions on Cognitive Communications and Networking*, vol. 11, no. 4, pp. 2340–2355, 2025.

[4] S. U. Khan, M. Kulhandjian, and D. Roy, "Pushing the Boundaries in CBRS Band: Robust Radar Detection within High 5G Interference," in *IEEE International Conference on Military Communications (MILCOM)*, October 2025, [Accepted].